Martian atmospheric CO_2 and pressure profiling with differential absorption lidar: System consideration and simulation results

Bing Lin and Zhaoyan Liu*

NASA Langley Research Center, Hampton, VA

*Contact information:

Zhaoyan Liu

MS 468, NASA Langley Research Center, Hampton, VA 23681, USA

Phone: 757-864-7192; Email: zhaoyan.liu@nasa.gov

Submitted to the Journal of Earth and Space Science

December 8, 2020

Abstract

This study explores a new concept of Martian differential absorption lidar operating at the 2-μm CO_2 absorption band for its atmospheric CO_2 and pressure observations. For the considered system, closely-spaced two or more wavelengths are selected so that environmental impacts such as surface reflection, atmospheric scattering, and absorptions from other trace gases on the lidar return signals are very similar for all selected wavelengths, but the difference in CO_2 absorption is substantial. Thus, Martian CO_2 amount and air pressure could be retrieved from the measured CO_2 differential absorption optical depth at the selected wavelengths. Simulations based on Mar's environmental conditions and technically available lidar systems show that lidar returns from the surface with horizontally 5 km averaging could have sufficient signal strengths that allow air barometry and CO_2 amount measurements with a noise induced random error (NIRE) smaller than 1% when the optical depth due to dust scattering, the dominant scatter in the Martian atmosphere, is 3 or less. In the presence of moderate dust aerosol loads and with the optimal selection of offline and online wavelengths, atmospheric CO_2 and pressure profiles could also be retrieved from the surface up to ~10 km altitude with the NIRE smaller than 1% for a horizontal resolution of 100 km and a vertical resolution of 100 m during night or 400 m during day. When a second online wavelength is use, the lidar would provide invaluable measurements of Martian CO_2 and pressure fields from surface up to about 13 km altitude.

1. Introduction

There are many factors affect states and dynamics of extraterrestrial planetary atmospheres of the solar system. Among these factors, atmospheric temperature and pressure may be the most important state variables in understanding the atmospheres. Generally, the atmospheric temperature structure is determined by thermodynamics especially the heating from solar and thermal radiation, while pressure and pressure gradient are the primary driving force for atmospheric motions that transport mass, heat and momentum (e.g., Holton 1979). Dry air movements of extraterrestrial planets are the most important atmospheric dynamic processes and controlled by radiative heating and pressure fields including horizontal and vertical pressure structures because these planets have much less water vapor in their atmospheres compared to Earth. For example, Martian atmosphere consists of most (about 95.32%) of carbon dioxide, and some nitrogen and argon (about 2.6% and 1.9%, respectively) along with traces of oxygen, water vapor, carbon monoxide, hydrogen, and other noble gases (Franz et al., 2017; Williams, 2020). The dry air processes transport mass and energy and generate clouds. Martian clouds are mostly of dust particles with small amounts of water ice and dry ice in the upper atmosphere. Thus, observation, modeling and prediction of temperature, pressure and cloud fields of Mars are critical in understanding of Martian weather systems, especially of Martian dust storms. These efforts would also provide great supports for safe and accurate atmospheric entry, landing site selection, and human colonization of Mars.

Global temperatures of planetary atmosphere and surface generally can be measured through infrared (IR) remotes sensing techniques. Although air pressure is extremely

important in characterizing dynamics of planetary atmosphere, spatial coverage of its observations is very limited even on Earth. For the Earth's atmosphere, currently only extremely sparse in-site measurements from buoys, ships, or dropsondes are available over open oceans. There are no global operational measurements of the pressure fields (Lin and Hu, 2005; Lawrence et al., 2011). For Martian atmosphere, the first surface air pressure measurements were made on some locations using in-situ barometers by the Viking Landers, Mars Pathfinder and recently InSight measurements (Banfield et al., 2020). Large scale surface air pressure mapping on Mars was available from Mars Express OMEGA visible and near infrared imaging spectrometer (Forget et al., 2007; Spiga et al., 2007). The passive remote sensing instrument measured CO_2 amount (actually CO_2 attenuation) from surface reflected solar radiation at the 2-μm CO_2 absorption band. Because of well mixtures of other gases and the domination of CO_2 in the Mars atmosphere, surface pressure fields were remotely sensed from the measured CO_2 (Forget et al., 2007; Spiga et al., 2007). For the CO_2 measurements, the impacts of solar insolation and albedo, dust optical properties, ice clouds, and frosts on the reflected 2-μm solar radiation were evaluated, which provided good control of retrieval quality (Spiga et al., 2007). The OMEGA surface air pressure retrievals revealed horizontal pressure gradients of Martian atmosphere, which led to observed inertia-gravity waves and convective cells of the atmosphere. Other processes such as pressure perturbations in the vicinity of topographical obstacles and seasonal surface pressure variations were obtained (Forget et al., 2007).

Although the surface pressure observations from passive remote sensing technique provides valuable insights for the dynamics of Martian atmosphere, it has certain

limitations. Critical issues with the passive technique for air pressure observations are: 1) the measurements can only be made during daytimes; 2) ranging capability is not possible, which potentially could lead systematic bias errors due to dust and cloud reflection that experiences different light path lengths compared to that of the surface reflection; and 3) observations are limited to surface pressure fields only and without sufficient information to account for surface elevation variations. To increase observational coverage and extend application limits, this study proposes to add active sensors to the current pressure sensing family for Martian atmospheric studies and Mars exploration. The considered instrument is a CO_2 differential absorption lidar (DIAL) for integrated path CO_2 amount measurements. This kind of DIAL systems has been developed, tested and applied for CO_2 measurements of the Earth's atmosphere for about a decade (Abshire et al., 2010; Lin et al., 2013; Dobler et al., 2013; Lin et al., 2015; Refaat et al., 2015, Singh et al., 2018; Campbell et al., 2020). The selected DIAL approach among those DIAL instrumentations for Earth is a pulsed system with wavelengths at the similar 2-μm CO_2 absorption band as OMEGA. Unlike passive sensors that can only provide columnar CO_2 measurements and the presence of clouds and aerosols can lead strong impacts on their measurements, a pulsed DIAL system with its inherited ranging capability can collect range-resolved return signals from all backscattering targets including aerosols, clouds and the surface. Therefore, it, along with an IR radiometer, can provide great potentials for vertical pressure and temperature profiling (Liu et al., 1999) and Martian cloud studies, similar to the CALIPSO mission for the Earth's atmosphere (Winker et al., 2009; Hunt et al., 2009). Also, a DIAL system will be suitable for pressure measurements of different topographical terrains and during

both day and night times. Our goal is to achieve a DIAL pressure measurement with an error within 1% which is compatible with or better than passive remote sensing and in-situ observations (Forget et al., 2007; Spiga et al., 2007).

Section 2 describes the basic concept of the DIAL approach, basic instrument structure and capability for CO_2 and pressure probing. In Section 3, simulation results for the considered system and its related CO_2 and pressure retrievals are presented. Finally, the conclusions are given in Section 4.

2. DIAL System and Methodology

2.1 DIAL system

Our CO_2 barometric lidar concept and instrumentation are based on measurements of differential absorption optical depth (DAOD) of two or more closely-spaced wavelengths at 2-μm CO_2 absorption band. These wavelengths are optimized to measure columnar CO_2 from Martian surface returns and to profile CO_2 from the atmospheric returns at low altitudes. Since there are multiple CO_2 absorption lines at the 2-μm band, these absorption lines are analyzed as the candidate for our DIAL system, which is very similar to pulsed systems used for CO_2 measurements of the Earth's atmosphere (Refaat et al., 2015). However, there are some significant differences between current Earth instruments and the considered Martian CO_2 lidar. First, compared to about 400 parts per million CO_2 volume mixing ratio in the Earth's atmosphere, the Martian atmosphere has abundant CO_2 (about 95.3% by volume) though its total amount of gases (or air pressure) is much lower. This causes the column CO_2 absorption at a given laser wavelength close to the center of a CO_2 absorption line is much stronger for Mars compared to that on

Earth. Secondly, the temperature and pressure of Martian atmosphere are both much lower than those of Earth, which significantly reduces absorption line broadening of gas absorption lines, enhances CO_2 absorption around line centers and quickly drops absorption strengths away from the line center. Thus, the considered lidar wavelengths should be at a wing of an absorption line to avoid excessive CO_2 absorption at line center that prevents the laser beam transmitting through the entire atmosphere and coming back. At the same time, these wavelengths should also provide sufficient differential absorption for an optimal CO_2 amount retrieval.

To quantitatively analyzing the CO_2 absorption features of the Martian atmosphere, spectral column CO_2 absorption optical depth (AOD) values as a function of wavelength, are calculated. For this calculation, the Orbiting Carbon Obervatory-2 spectroscopic model (i.e., the ABSCO Table (Thompson et al., 2012; Payne et al., 2017)) is used. The Martian atmospheric climatology of temperature and pressure profiles is obtained from the Viking mission (Seiff and Kirk, 1977). The basic features of the climatology include specified surface temperature and pressure 224 K and 663 Pa, respectively, temperature lapse rate about 1.5 K/km and scaleheight about 11 km.

From the requirements of wavelength selection mentioned previously and the features of Martian atmosphere, spectral analysis leads us the selection of the same CO_2 absorption line (line center at 2050.428 nm) within the 2-μm band for our instrumentation as those used in lidar systems for Earth (Refaat et al., 2015). However, the exact online and offline wavelengths of the laser for the considered Martian differential absorption lidar are different. For example, the offline wavelength selected here for Martian atmosphere is even slightly closer to the absorption line center compared

to the online wavelength of the lidar for the Earth's atmosphere due to much weaker broadening of the CO_2 absorption line within the Martian atmosphere. The two online wavelengths (called primary and secondary online wavelengths) are even shorter and closer to the line center.

Figure 1 shows the spectral characteristics of CO_2 AOD from the top-of-atmosphere (TOA) to surface at the considered wave band. The AOD cutoff for wavelengths around the absorption line center in the figure is to avoid the extreme high values (about 2200). The red star on right is for the offline wavelength (2050.508 nm), while the two red stars from left are for the secondary (2050.437 nm) and primary (2050.441 nm) online wavelengths, respectively. The AOD values at these online and offline wavelengths are dominantly caused by the absorption of the strong absorption line and may have very limited influences from weaker lines around. The one-way CO_2 DAOD value for the pair of the primary online and offline is optimized to be 1.11 at ~3 km altitude. The details on the optimal wavelength selection of differential absorption lidars can be seen from the discussions of the subsection 2.4 (also c.f., Lin et al., 2013, 2017; Dobler et al., 2013). The DAOD value for the pair of the secondary online and offline is about 2 times higher than that of primary online pair, which provides a better profiling capability for atmospheric pressures at higher altitudes. Although surface pressure is the most important pressure value needed for dynamics, this optimization at ~3 km above the surface can provide best coverage of the lower atmosphere as well as the surface. Lidar return signals from arid surface are generally much stronger than that from the atmosphere and, thus, the considered CO_2 DIAL system has sufficiently strong return

signals from the surface to achieve high precision and accuracy in surface barometry (c.f., discussions in the subsection 2.4).

Figure 2 shows vertical profiles of (a) the absorption optical depth (AOD) values from top-of-atmosphere (TOA) to the specified altitude for the considered three wavelengths, and (b) the normalized weighted mean differential absorption cross sections of the two wavelength pairs for entire atmospheric column CO_2 measurements. The offline AOD values are very small, even for the value (~0.06) from TOA to surface, and only about 1/20 of those from primary online wavelength. The AOD values for both online wavelengths increase quickly with decreasing altitudes, especially at the lowest part (from 0 to ~10 km altitudes) of troposphere (note the logarithm scale is used in Fig. 2a). The CO_2 absorption at secondary online wavelength is about twice as strong as that of primary online wavelength. The very similar character of the two weighted differential absorption cross section values is the result of the location of selected wavelengths and normalization of the mean absorption cross sections (i.e., a factor of two, nearly constant proportionality in CO_2 absorption strengths for the secondary pair compared to the primary pair). All online wavelengths are located at near linear portion of the wing of the CO_2 absorption line as illustrated in Figure 1. When normalizing or scaling linearly the weighted differential absorption values of the two wavelength pairs, almost the same results are obtained. The two pairs of DAOD measurements both have strong weighting for lowest Martian atmosphere, especially below the scaleheight of the Martian atmosphere, as shown in their weighted values. Thus, with the considered DIAL system, Mars' surface and lowest atmospheric pressure fields could be measured properly. Additionally, dust and cloud optical properties could be retrieved from the

DIAL lidar profiles like the case of the CALIPSO lidar for the Earth's atmosphere using offline lidar signal returns (Liu et al., 2009; Winker et al., 2009; Hunt et al., 2009).

From an engineering point of view, the wavelength selection and system consideration are feasible for instrument development. The wavelength separation between primary online and offline wavelengths is about 67 picometer (pm), while the separation of two online wavelengths is about 3.7 pm. These separations are very close to what used in airborne and previously considered spaceborne CO_2 DIAL systems (Lin et al., 2013; Dobler et al., 2013). In terms of stabilizing wavelength selected, the line centers of both the strong line considered here and the weak absorption line between the online and offline wavelengths centered at about 2050.483 nm (Fig. 1) can be used in wavelength locking loop as done by current CO_2 systems (Abshire et al., 2010, Dobler et al., 2013; Refaat et al., 2015). To achieve 1% accuracy of DAOD measurement, the knowledge on laser frequency variations is required to be better than 2.6 MHz. Such a requirement to the frequency stability has already been achieved by CO_2 lidars for Earth observations. Current Earth observing systems reach high precise CO_2 observations (total uncertainty < 1 ppm for 400 ppm CO_2 volume mixing ratio of the Earth's atmosphere or a relative error < 0.25%) by a combination of wavelength locking and wavelength variation recording techniques (Dobler et al., 2013; Lin et al., 2013; Campbell et al., 2020).

For the laser power consideration, the Martian atmosphere is more favorable to the CO_2 measurement because of the following reasons. (1) It does not have additional water vapor absorption like the Earth's atmosphere for the selected wavelengths, and hence CO_2 retrieval algorithms can be simplified compared to those for Earth. (2) The

reflectance of Martian surface is high due to entire desertification, which provides strong surface reflected signals for the column CO_2 measurements. (3) The background noise level caused by solar radiation is much weaker for Martian DIAL system compared that for the Earth CO_2 lidars because Mars is significantly further away from the sun compared to Earth. (4) The orbiting altitude on Mars could be as low as ~240 km. This would provide a factor of ~9 increase in the lidar return signals compared with the satellite-born lidars on Earth such as the CALIPSO lidar which has a nominal orbiting altitude of ~705 km (Winder et al., 2009). And, (5) more importantly, dust aerosols on Mars are ubiquitous and can extend vertically up to 40 km or even higher and would be ideal backscatter target for CO_2 profiling. These factors could save the power, size, telescope, and cost of Martian lidars compared to those for Earth. That is, the similar systems for Earth could be directly adopted to Mars' applications. Figure 3 illustrates the conceptual design of the considered instrument. The laser source (seed) provides base laser wavelengths. It is modulated and locked to needed wavelengths. The laser powers at these wavelengths, then, are amplified and transmitted to the atmosphere. A very small portion of the laser beam is split and sent to power monitoring detector as reference to normalize lidar transmitted powers at individual wavelengths and account for potential laser energy variations. The backscattered lidar return signals from the atmosphere and surface are collected by the lidar receiving telescope and, then, detected, amplified and digitized for data acquisition. Such a CO_2 DIAL system is very similar to current instruments for Earth's CO_2 measurements (Dobler et al., 2013; Lin et al., 2013; Refaat et al., 2015). Thus, there is a high chance of success in development of the considered CO_2 DIAL system for Martian atmosphere applications.

2.2 Methodology

The received lidar return signal at a given wavelength from the Martian atmosphere, in photoelectrons, can be written as (Liu et al., 2000):

$$N_s = \frac{1}{r^2}\frac{c\Delta t}{2}C_0\left[\beta_M(r)+\beta_P(r)\right]\exp\left[-2\left(\tau_{CO_2}(r)+\tau_{other}(r)\right)\right], \quad (1)$$

or from the surface

$$N_s = \frac{1}{r^2}C_0 R_{surf}\exp\left[-2\left(\tau_{CO_2}(r)+\tau_{other}(r)\right)\right], \quad (2)$$

where β_M is the Rayleigh backscattering coefficient from molecules which can be ignored for the Martian atmosphere at 2-μm wavelengths and β_P represents the particulate backscattering coefficients from the dust aerosols or clouds at range r from the lidar. They can be approximately calculated using Mie and T-Matrix scattering theories because of their small particle sizes or obtained from CALIPSO observations based on Earth's atmosphere. R_{surf} is the surface reflectivity in sr^{-1}. $\tau_{CO2}(r)$ and $\tau_{other}(r)$ are the optical depth due to the CO_2 absorption and any atmospheric agents other than CO_2 (mainly the particulate scattering due to dust and ice cloud) along the laser beam from the lidar to r. Δt is the sampling time, and c the speed of light. C_0 is the lidar constant that contains lidar system parameters and other range-independent quantities. It can be written as:

$$C_0 = E_0 A_0 k_o \eta_Q \frac{\lambda}{hc} \quad (3)$$

Here, E_0 is the laser output energy per pulse, A_0 is the receiving telescope area, k_0 the optical throughput of the lidar transceiver, and λ the laser wavelength. η_Q is the quantum

efficiency of the detector, and h the Planck's constant. C_0 is determined using the return signal from target whose scattering property is known.

For the CO_2 differential absorption measurement, a typical practice is to select two (Lin et al., 2013), three (Rafaat et al., 2015) or multiple wavelengths (Abshire et al., 2010) at a CO_2 absorption line. One wavelength is chosen far off the center of the absorption line so that the absorption is insignificant and is used as a reference (called offline). The other wavelengths (called online) are selected on the line where the absorption is significant such that CO_2 can be well measured. The selected wavelengths are very close, therefore the scattering optical depths at these wavelengths only differ very slightly, that is, τ_{other} almost does not change at these selected wavelengths. Taking ratio of the lidar return signals at online and offline wavelengths,

$$\frac{N_{s,on}}{N_{s,off}} = \frac{C_{on}}{C_{off}} \exp\left(-2\left(\tau_{CO_2,on} - \tau_{CO_2,off} + \tau_{other,on} - \tau_{other,off} \right) \right) = \frac{C_{on}}{C_{off}} \exp\left(-2\left(\Delta\tau_{CO_2} + \Delta\tau_{other} \right) \right)$$

, (4)

we can derive the differential optical depth as:

$$\Delta\tau_{CO_2} + \Delta\tau_{other} = -\frac{1}{2} \ln\left(\frac{N_{s,on}}{N_{s,off}} \frac{C_{off}}{C_{on}} \right). \quad (5)$$

$\Delta\tau_{other}$ is the differential optical depth due to all atmospheric agents other than CO_2. It is mainly due to the scattering by airborne dust and/or ice clouds in the Martian atmosphere. Because the selected online and offline wavelengths are very close, $\Delta\tau_{other}$ is negligibly small and can be corrected or removed. The CO_2 differential absorption optical depth (DAOD) can be further written as:

$$\Delta\tau_{CO_2} = \int_z^{TOA} \left[\alpha_{CO_2,on}(z') - \alpha_{CO_2,off}(z')\right] n_{CO_2}(z')\, dz' = A_{CO_2}(z)\, N_{CO_2}(z), \quad (6)$$

where α_{CO2} *(z)* and n_{CO2} *(z)* are the CO_2 absorption cross section and number density at altitude *z*, respectively. N_{CO2} *(z)* is the column CO_2 number from *z* to TOA. *A(z)* is a weighted mean differential absorption cross section from *z* to TOA and can be calculated using a spectroscopic model along with atmospheric profiles of temperature, pressure and gas number density. That is,

$$A_{CO_2}(z) = \frac{\int_z^{TOA} \left[\alpha_{CO_2,on}(z') - \alpha_{CO_2,off}(z')\right] n_{CO_2}(z')\, dz'}{\int_z^{TOA} n_{CO_2}(z')\, dz'}. \quad (7)$$

From Eq. (6), we derive

$$N_{CO_2}(z) = \frac{\Delta\tau_{CO_2}(z)}{A_{CO_2}(z)}, \quad (8)$$

and this molecular number decides the air pressure caused by CO_2:

$$P_{CO_2}(z) = M_{CO_2} g_W(z)\, N_{CO_2}(z), \quad (9)$$

where M_{C02} is the CO_2 molecular mass, and

$$g_W(z) = \int_z^{TOP} g(z') n_{CO_2,\mathrm{model}}(z')\, dz' \quad (10)$$

is a weighted mean Martian gravitational acceleration between *z* and TOA, *g(z)* the gravitational acceleration at altitude *z* in a specific latitude. This CO_2 air pressure dominates Martian atmospheric pressure fields. Since the amounts of other gases in Martian atmosphere are minor and either very stable or negligible, the total air pressure can be obtained from the summation of this CO_2 pressure and the air pressure introduced by all other gases. From the ideal gas law, the atmospheric temperature can also be

derived if the molecular scattering signal is measured (Liu et al., 1999). Similar idea could be applied to the DIAL measurement. However, our simulations showed that, to make accurate temperature measurement for the Mars DIAL system considered in this study, an average over thousands of kilometers along the track is necessary which make the temperature measurement impractical. Fortunately, temperature could be measured with IR radiometers as mentioned earlier.

2.3 Random error analysis

Based on the first order error propagation theory, the error ε and the relative error due to random noise for all individual quantities in Eqs. (6) – (11) can be estimated (Ehret et al., 2008; Kameyama et al., 2011; Lin et al., 2013) using:

$$\varepsilon_{\Delta\tau_{CO_2}} = \frac{1}{2}\left(\left(\frac{1}{SNR_{on}}\right)^2 + \left(\frac{1}{SNR_{off}}\right)^2\right)^{1/2} \tag{11a}$$

$$\frac{\varepsilon_{\Delta\tau_{CO_2}}}{\Delta\tau_{CO_2}} = \frac{1}{2\Delta\tau_{CO_2}}\left(\left(\frac{1}{SNR_{on}}\right)^2 + \left(\frac{1}{SNR_{off}}\right)^2\right)^{1/2}, \tag{11b}$$

$$\varepsilon_{n_{CO_2}}(z) = \frac{\varepsilon_{\Delta\tau_{CO_2}}(z)}{A(z)}, \tag{12a}$$

$$\frac{\varepsilon_{N_{CO_2}}(z)}{N_{CO_2}} = \frac{\varepsilon_{\Delta\tau_{CO_2}}(z)}{\Delta\tau_{CO_2}(z)}, \tag{12b}$$

$$\varepsilon_{P_{CO_2}}(z) = M_{CO_2} g_W(z)\, \varepsilon_{N_{CO_2}}(z), \tag{13a}$$

$$\frac{\varepsilon_{P_{CO_2}}(z)}{P_{CO_2}(z)} = \frac{\varepsilon_{N_{CO_2}}(z)}{N_{CO_2}(z)} = \frac{\varepsilon_{\Delta\tau_{CO_2}}(z)}{\Delta\tau_{CO_2}(z)} \tag{13b}$$

These results clearly show that the relative errors in measured CO_2 differential absorption optical depth are equivalent to their corresponding relative errors of CO_2 amount and air pressure observations for current DIAL approach. Thus, most analysis hereafter is focused on the CO_2 differential absorption optical depth.

2.4 Wavelength optimization

In order to have the best performance of the CO_2 DIAL system, optimal selection of laser wave lengths is considered. This wavelength optimization is to minimize the relative error in CO_2 DAOD retrievals. From Eq. (11b), we further obtain:

$$\begin{aligned}\frac{\varepsilon_{\Delta\tau_{CO_2}}}{\Delta\tau_{CO_2}} &= \frac{1}{2\Delta\tau_{CO_2}}\left(\left(\frac{1}{SNR_{on}}\right)^2 + \left(\frac{1}{SNR_{off}}\right)^2\right)^{1/2} \\ &= \frac{1}{\Delta\tau_{CO_2}}\frac{z}{2\sqrt{C}}\left(\frac{1}{\exp\left(-2\left(\tau_{CO_2 on}+\tau_d\right)\right)} + \frac{1}{\exp\left(-2\left(\tau_{CO_2 off}+\tau_d\right)\right)}\right)^{1/2} \\ &= \frac{1}{\Delta\tau_{CO_2}}\frac{z}{2\sqrt{C}}\left(\exp(2\Delta\tau_{CO_2})+1\right)^{1/2}\exp\left(\tau_{CO_2 off}+\tau_d\right)\end{aligned} \tag{14}$$

Take derivative of Eq. (14) on CO_2 differential absorption optical depth and set the result to be 0, we have:

$$\begin{aligned}&\frac{d}{d\Delta\tau_{CO_2}}\left(\frac{\left(\exp(2\Delta\tau_{CO_2})+1\right)^{1/2}}{\Delta\tau_{CO_2}}\right) \\ &= -\frac{\left(\exp(2\Delta\tau_{CO_2})+1\right)^{1/2}}{\Delta\tau_{CO_2}^{\ 2}} + \frac{\frac{1}{2}\left(\exp(2\Delta\tau_{CO_2})+1\right)^{-1/2}2\exp(2\Delta\tau_{CO_2})}{\Delta\tau_{CO_2}} = 0\end{aligned}, \tag{15}$$

Thus, we have obtained the following transcendental equation:

$$\exp\left(2\Delta\tau_{CO_2}\right)\left(1-\Delta\tau_{CO_2}\right)+1=0 \quad (16)$$

The root of this transcendental equation $\Delta\tau_{CO2}$ is about 1.11.

For Marian atmospheric applications, the lidar measurement is optimized at ~3 km altitude by selecting the primary wavelength so that the DAOD from TOA to 3 km is 1.11. This selection of 3 km altitude provides a good coverage of the measurement over the lower atmosphere (from the surface to ~10 km) for a moderate dust load (c.f., Section 3). For the measurement from the secondary online wavelength, the optimization is designed to be located at ~8 km altitude. A combination of the two lidar wavelength pairs would provide invaluable measurements of Martian atmospheric CO_2 and pressure fields from surface up to about 13 km altitude, the most important layer for Martian atmospheric dynamics.

3. Simulation Results

Observing system simulation experiments (OSSEs) are performed based on the system parameters in Table 1. The detector is assumed to be a DRS APD for spaceborne lidar application (Lin et al., 2013; Sun et al., 2017). The system optical parameters including the telescope, field of view (FOV), beam expander, and transceiver throughputs are adapted from the CALIPSO lidar (Hunt et al., 2009). An optical interference filter is assumed for solar radiation blocking. The laser sources could be a single-frequency fiber laser, or a fiber maser laser and crystal amplifier system operated at individual wavelengths.

Table 1 Parameters used in OSSEs

Laser	pulse energy, online / offline (mJ)	5 / 2
	pulse repetition frequency (Hz)	2000
	beam expander throughput	0.883
	Wavelengths: primary, secondary, and offline (nm)	2050.44156, 2050.43779, 2050.50812
Telescope	diameter (m)	1
	clear area ratio	0.882
Detector (DRS APD)	net quantum efficiency	0.68
	dark current (A)	3.5e-13
	gain	900
Lidar receiver FOV (mrad)		0.13
Solar blocking filter bandwidth (nm)		0.2
System optical throughput		0.325
Surface reflectivity (sr^{-1})		0.161
Satellite altitude (km)		240

The OSSE results are presented in Fig. 4. Fig. 4a is the dust profile, modeled based on the dust vertical distribution observed by the SPICAM occultation measurement on Mars-Express (Fedorova et al., 2009). The occultation measurement was made above 10 km, and we extrapolated the dust distribution to the surface, following the observed exponential curve. The modeled dust column optical depth (OD) from TOA to the surface is 0.373. Dust on Mars shows strong annual and geophysical variability (Smith et al., 2004). Dust OD can change from ~0.4 to ~1.4 at 880 nm (Chen-Chen et al., 2019) and was as large as ~8 during the Mars year 34 global dust storm (Guzewich, et al., 2019). Global long-term lidar observations of the Martian atmosphere would gain our knowledge on the dust variability. The dust model in Fig. 4a is for Martian climatological dust loading conditions. When the dust loading increases, the lidar return signal becomes larger and a larger vertical coverage is achievable in the atmosphere. For heavy dust loading cases, we expect the considered lidar would only probe into upper

part of the dust systems till OD about 2 ~ 3 level as demonstrated by the CALIPSO mission.

Fig. 4b shows that the noise induced random error (NIRE) in simulated measurements of CO_2 DAOD to the surface at a horizontal 5 km resolution increases as the dust OD increases, and is smaller than 1% until the dust OD reaches ~3 for both night- and day-time measurements because the lidar signal decreases exponentially with dust OD and the surface return signal shot noise is the dominant random error source. It also can be noticed that when dust OD is less than 1, the errors in column CO_2 and surface air pressure measurements are much (more than an order of magnitude) less than 1%. In other words, the measurements can achieve the 1% error requirement with a much-reduced laser pulse energy and/or the telescope size, if the measurement is focused only on the surface pressure and column CO_2. This measurement error character also holds for the column CO_2 molecule numbers and surface air pressure (c.f., Eq. 13b). In the atmosphere (Figs. 4 c and d), more average both horizontally and vertically is necessary to achieve 1% NIRE, because the dust backscatter coefficient is much smaller than the surface reflectivity. The signal-to-noise ratio (SNR) values of nighttime lidar returns are very encouraging and larger than 100 from the surface up to about 15 km for the offline wavelength through 100m vertical integration and 100km horizontal averaging (Fig. 4c). For online wavelengths, the high SNR values are maintained from 20 km down to about 10 km altitudes. After that, though the SNR of lidar signals gets smaller, relative errors in CO_2 measurements could keep small because AOD values increase sharply (c.f., Fig. 2a). Measurements of the CO_2 molecule number and air pressure could be made with the pair of primary online and offline wavelengths with 1% NIRE up to ~10 km at a

horizontal resolution of 100 km and vertical resolution of 100 m during night and 400 m during day (c.f., Fig. 4d). With the secondary online wavelength pair, the measurements could be extended to even higher (~13km) altitudes. Thus, with the laser energies and system parameters in Table 1, the lidar return can be collected with a descent SNR to allow measurements of column CO_2 amount and pressure over the surface and within low atmosphere.

4. Conclusions

This study proposes a novel concept in use of a differential absorption barometric lidar operating at the 2 μm CO_2 absorption complex to remotely sense Martian atmospheric CO_2 amount and air pressure. The considered CO_2 lidar system is very similar to what developed for precise observations of Earth's atmospheric CO_2, and can be basically developed from the existing CO_2 lidar technology. The system is designed to have an offline and two online (primary and secondary) wavelengths. Based on the Mar's observed environmental conditions, technically available laser systems and optimal selection of lidar online and offline wavelengths proposed here, this study shows that the considered CO_2 lidar can enable CO_2 and pressure measurements from the surface to the atmosphere up to about 13 km altitude when relative errors within 1% of the concerned quantities are required. This 1% error requirement is similar to or less than those of current Martian in-situ and passive remote sensing observations and meets general Mar's dynamic and climate science needs. Thus, the considered lidar remote sensing will provide crucial dynamic information for Martian weather and climate systems in future Mars explorations.

Current study is an initial effort on active Martian atmospheric CO_2 remote sensing. More efforts on Mars' instrumentation development and exploring Mar's CO_2 measurements for broad science applications such as Martian atmospheric entry, landing site selection, severe dust storm prediction, and Mars' colonization are needed in future work.

Acknowledgement

We would like to thank the NASA Langley Research Center for its supports on this study. Special thanks to J. Yu and L. Petway for their insights on the 2-μm technology development, and K. Powell for useful discussion on the CALIPSO lidar measurement simulation.

Reference

Abshire, J. B., H. Riris, G. R. Allan, C. J. Weaver, J. Mao, X. Sun, W. E. Hasselbrack, S. R. Kawa, and S. Biraud, Pulsed airborne lidar measurements of atmospheric CO_2 column absorption, *Tellus B*, *62*(5), 770–783, 2010.

Banfield, D., et al., The atmosphere of Mars as observed by InSight, Nature Geoscience, 13, 190–198, 2020. https://doi.org/10.1038/s41561-020-0534-0

Campbell, J., B. Lin, E. Browell, M. Obland, J. Dobler, W. Erxleben, D. McGregor, C. O'Dell, E. Bell, S. Pal, B. Weir, T. Fan, S. Kooi, A. Corbett, K. Davis, I. Gordon, R. Kochanov, Field Evaluation of Column CO_2 Retrievals from Intensity-Modulated Continuous-Wave Differential Absorption Lidar Measurements during ACT-America, Earth and Space Science, 2020 (DOI: 10.1029/2019EA000847).

Chen-Chen, H., S. Pérez-Hoyos, and A. Sánchez-Lavega, Dust particle size and optical depth on Mars retrieved by the MSL navigation cameras, Icarus, 319, 43-57, 2019.

Dobler, J. T., F. W. Harrison, E. V. Browell, B. Lin, D. McGregor, S. Kooi, Y. Choi, and S. Ismail, Atmospheric CO_2 column measurements with an airborne intensity-modulated continuous wave 1.57 μm fiber laser lidar, Applied Optics, 52 (12), 2874-2892, 2013.

Ehret, G., C. Kiemle, M. Wirth, A. Amediek, A. Fix, and S. Houweling, Satellite-borne remote sensing of CO_2, CH_4, and N_2O by integrated path differential absorption lidar: a sensitivity analysis, Appl. Phys. B 90, 593–608, 2008.

Fedorova, A., O. Korableva, J.-L. Bertauxb, A.V. Rodina, F. Montmessin, D.A. Belyaeva, A. Reberac, Solar infrared occultation observations by SPICAM

experiment on Mars-Express: Simultaneous measurements of the vertical distributions of H2O, CO2 and aerosol, Icarus, 200, 96–117, 2009.

Forget, F., A. Spiga, B. Dolla, S. Vinatier, R. Melchiorri, P. Drossart, A. Gendrin, J.-P. Bibring, Y. Langevin, and B. Gondet, Remote sensing of surface pressure on Mars with the Mars Express/OMEGA spectrometer: 1. Retrieval method, J. Geophys. Res., doi:10.1029/2006JE002871, 2007.

Franz, H.; M. Trainer, C. Malespin, P. Mahaffy, S. Atreya, R. Becker, M. Benna, P. Conrad, J. Eigenbrode, Initial SAM calibration gas experiments on Mars: Quadrupole mass spectrometer results and implications. Planetary and Space Science. 138: 44–54, 2017, Bibcode:2017P&SS44F. doi:10.1016/j.pss.2017.01.014. ISSN 0032-0633.

Guzewich, S. D., Lemmon, M., Smith, C. L., Martínez, G., de Vicente-Retortillo, Á., Newman, C. E., et al., Mars Science Laboratory observations of the 2018/Mars year 34 global dust storm. Geophysical Research Letters, 46, 71–79, https://doi.org/10.1029/2018GL080839, 2019.

Holton, J., An Introduction to Dynamic Meteorology, 3rd edition, *Academic Press*, 1992.

Hunt, W., D. Winker, M. Vaughan, K. Powell, P. Lucker, and C. Weimer: CALIPSO lidar description and performance assessment. J. Atmos. Oceanic Technol., 26, 1214–1228, 2009.

Kameyama, S., M. Imaki, Y. Hirano, S. Ueno, S. Kawakami, D. Sakaizawa, T. Kimura, and M. Nakajima, Feasibility study on 1.6 μm continuous-wave modulation laser absorption spectrometer system for measurement of global CO_2 concentration from a satellite, Appl. Opt. 50, 2055–2068, 2011.

Lawrence, R., B. Lin, S. Harrah, Y. Hu, P. Hunt, and C. Lipp, Initial flight test results of differential absorption barometric radar for remote sensing of sea surface air pressure, 112, 247-253, JQSRT, 2011.

Lin, B, S. Ismail, F. W. Harrison, E. V. Browell, A. R. Nehrir, J. Dobler, B. Moore, T. Refaat, and S. A. Kooi, Modeling of intensity-modulated continuous-wave laser absorption spectrometer systems for atmospheric CO_2 column measurements, Applied Optics, 52 (29), 7062-7077, 2013.

Lin, B., A. Nehrir, F. Harrison, E. Browell, S. Ismail, M. Obland, J. Campbell, J. Dobler, B. Meadows, T. Fan, and S. Kooi, Atmospheric CO_2 column measurements in cloudy conditions using intensity-modulated continuous-wave lidar at 1.57 micron, Optics Express, 23, DOI:10.1364/OE.23.00A582, A582 – A593, 2015.

Lin, B., and Q. Min, Optimal frequency selection of multi-channel O_2-band differential absorption barometric radar for air pressure measurements, Journal of Quantitative Spectroscopy & Radiative Transfer, 188, 188–191, 2017. (http://dx.doi.org/10.1016/j.jqsrt.2016.06.019).

Lin, B., and Y. Hu, Numerical simulations of radar surface air pressure measurements at O_2 bands, Geoscience Remote Sens. Lett., 2, 324-328, 2005.

Liu, Z., I. Matsui, and N. Sugimoto, High-spectral-resolution lidar using an iodine absorption filter for atmospheric measurements, Opt. Eng. 38, 1661–1670, 1999.

Liu, Z., M. A. Vaughan, D. M. Winker, C. Kittaka, R. E. Kuehn, B. J. Getzewich, C. R. Trepte, and C. A. Hostetler. The CALIPSO Lidar Cloud and Aerosol Discrimination: Version 2 Algorithm and Initial Assessment of Performance, J.

Atmos. Oceanic Technol., 26, 1198-1213, https://doi.org/10.1175/2009JTECHA1229.1, 2009.

Liu, Z., P. Voelger, and N. Sugimoto, Simulations of the observation of clouds and aerosols with the Experimental Lidar in Space Equipment system, Appl. Opt., 39, 3120-3137, 2000.

Payne, V., ABSCO User Guide, Jet Propulsion Laboratory, CA, July 24, 2017. (https://docserver.gesdisc.eosdis.nasa.gov/public/project/OCO/ABSCO_UsersGuide_20170724_corr2_v5.0.pdf).

Refaat, T., U. Singh, J. Yu, M. Petros, S. Ismail, M. Kavaya,1 and K. Davis, Evaluation of an airborne triple-pulsed 2 μm IPDA lidar for simultaneous and independent atmospheric water vapor and carbon dioxide measurements, Appl. Opt., 54, 1387–1398, 2015.

Seiff, A., and D. Kirk, Structure of the atmosphere of Mars in summer at mid-latitudes, JGR, 28, 4364-4378, 1977.

Singh, U., T. Refaat, M. Petros, and S. Ismail, Evaluation of 2-μm Pulsed Integrated Path Differential Absorption Lidar for Carbon Dioxide Measurement—Technology Developments, Measurements, and Path to Space, IEEE Journal Of Selected Topics in Applied Earth Observations and Remote Sensing, 11, 2059 – 2067, 2018.

Smith, M. D., Interannual variability in TES atmospheric observations of Mars during 1999–2003, Icarus, 167, 148–165, 2004.

Spiga, A., F. Forget, B. Dolla, S. Vinatier, R. Melchiorri, P. Drossart, A. Gendrin, J.-P. Bibring, Y. Langevin, and B. Gondet, Remote sensing of surface pressure on Mars

with the Mars Express/OMEGA spectrometer: 2. Meteorological maps, J. Geophys. Res., 112, E08S16, doi:10.1029/2006JE002870, 2007.

Sun, X., J. B. Abshire, J. D. BECKBeck, P. Mitra, K. Reiff, and G. Yang, HgCdTe avalanche photodiode detectors for airborne and spaceborne lidar at infrared wavelengths, Optics Express, 26, 16589-16602, 2017.

Thompson, D., et al., Atmospheric validation of high accuracy CO_2 absorption coefficients for the OCO-2 mission, Journal of Quantitative Spectroscopy & Radiative Transfer, 113, 2265–2276, 2012.

Williams, D., Mars Fact Sheet, Last updated on 15 June 2020. (https://nssdc.gsfc.nasa.gov/planetary/factsheet/marsfact.html.)

Winker, D. M., M. A. Vaughan, A. Omar, Y. Hu, K. A. Powell, Z. Liu, B. Hunt, and S. Young, Overview of the CALIPSO Mission and CALIOP Data Processing Algorithms, Journal of Atmospheric and Oceanic Technology, 26, 2310-2323, 2009.

Figure Captions

Figure 1. Spectral characteristics at the 2050 CO_2 absorption band. Plotted values are for CO_2 absorption optical depth (AOD) from TOA to surface. The extreme high values around the absorption line center are out-of-scale and not shown. The red star on right is for the offline wavelength, while the two red stars from left are for the secondary and primary online wavelengths, respectively.

Figure 2. Vertical profiles of (a) AOD values from TOA to a specified altitude for the three selected wavelengths, and (b) the normalized weighted mean differential absorption cross section values of the two wavelength pairs for entire atmospheric column CO_2 measurements.

Figure 3. The conceptual design of Martian CO_2 DIAL instrument.

Figure 4. The simulation results: (a) dust profile modeled based on the dust vertical distribution observed by the SPICAM occultation measurement on Mars-Express; (b) the noise induced random error (NIRE) in CO_2 DAOD to the surface at a horizontal 5 km resolution; (c) nighttime lidar signal-to-noise ratios (SNR) for horizontal 100 km and vertical 100m averages; and (d) relative error profiles of DAOD retrievals for the two wavelength pairs and day and night times as indicated in the panel.

Figure 1.

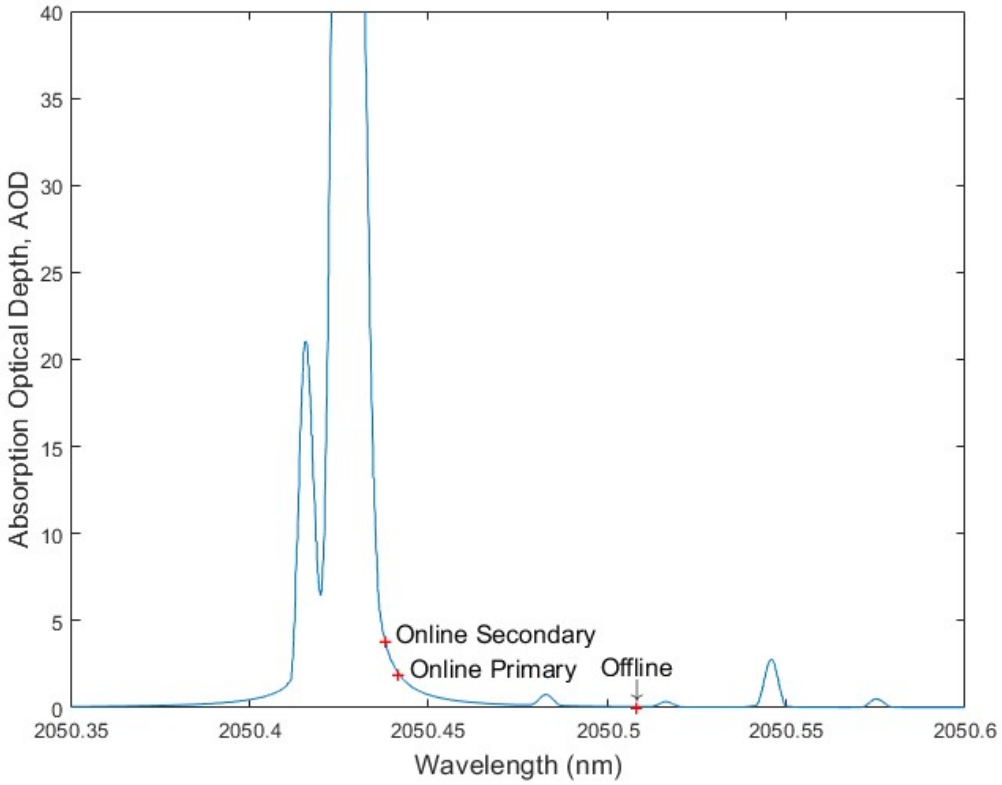
Absorption Optical Depth, AOD
Wavelength (nm)
Online Secondary
Online Primary
Offline
0
5
10
15
20
25
30
35
40
2050.35
2050.4
2050.45
2050.5
2050.55
2050.6

Figure 2.

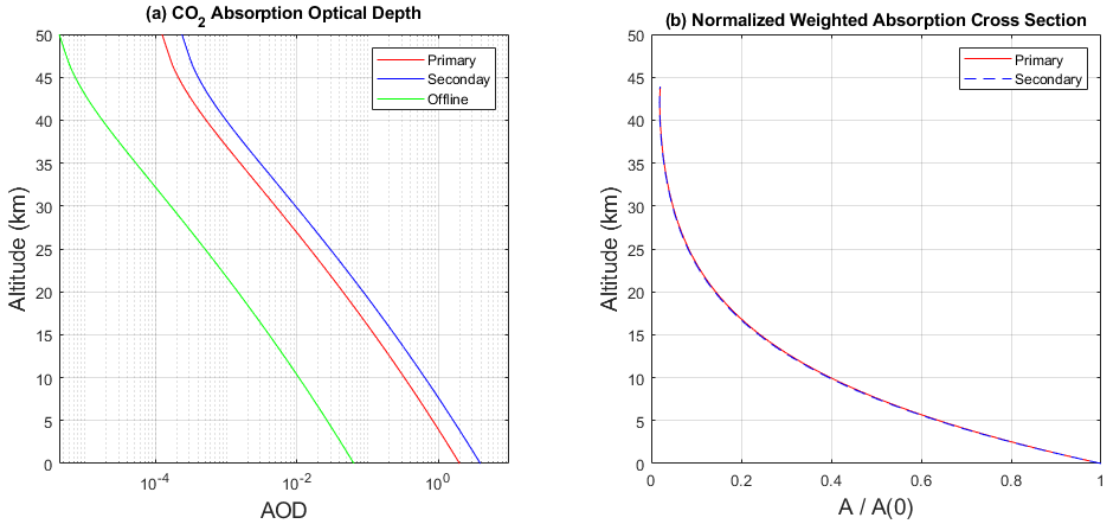
(a) CO2 Absorption Optical Depth
Primary
Seconday
Offline
Altitude (km)
AOD
(b) Normalized Weighted Absorption Cross Section
Primary
Secondary
Altitude (km)
A / A(0)

Figure 3.

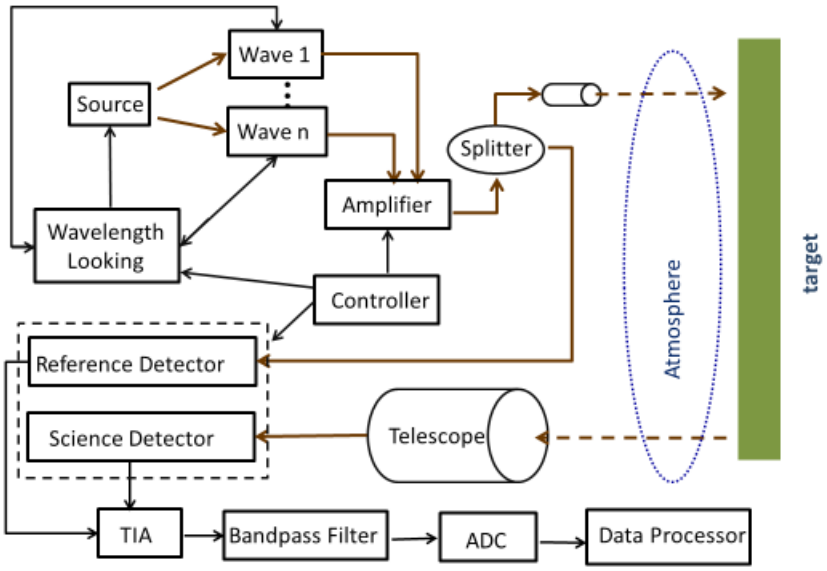

Figure 4.

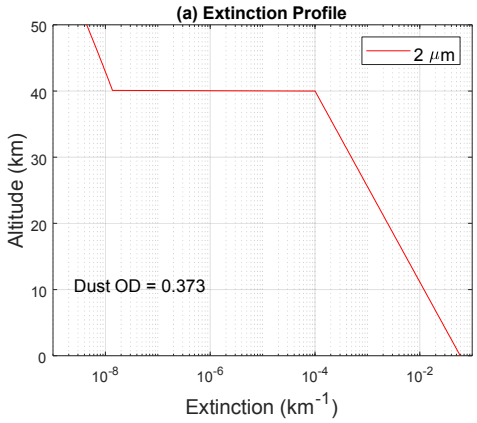
(a) Extinction Profile
2 μm
Dust OD = 0.373
Altitude (km)
Extinction (km^-1)

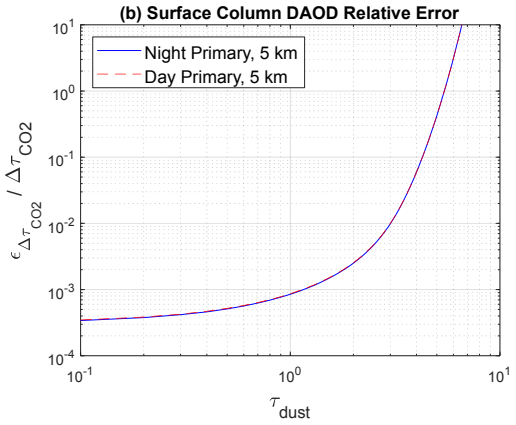
(b) Surface Column DAOD Relative Error
Night Primary, 5 km
Day Primary, 5 km
τdust

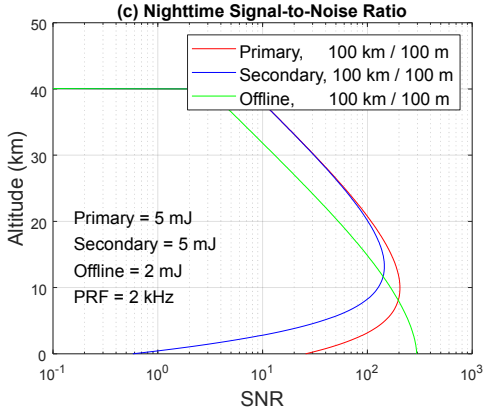
(c) Nighttime Signal-to-Noise Ratio
Primary, 100 km / 100 m
Secondary, 100 km / 100 m
Offline, 100 km / 100 m
Primary = 5 mJ
Secondary = 5 mJ
Offline = 2 mJ
PRF = 2 kHz
Altitude (km)
SNR

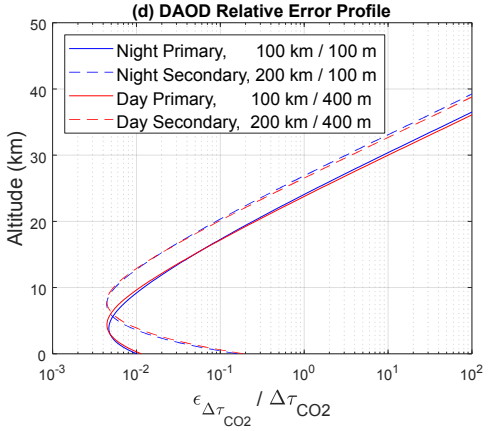
(d) DAOD Relative Error Profile
Night Primary, 100 km / 100 m
Night Secondary, 200 km / 100 m
Day Primary, 100 km / 400 m
Day Secondary, 200 km / 400 m
Altitude (km)